Numerical study of the behavior of the bolted shear connection in cold-formed steel-concrete composite beam

Žuvelek, Vlaho; Ćurković, Ivan; Lukačević, Ivan; Rajić, Andrea

CFSRC COLLOQUIUM

Proceedings of the Cold-Formed Steel Research Consortium Colloquium
17-19 October 2022 (cfsrc.org)

Numerical study of the behavior of the bolted shear connection in cold-formed steel-concrete composite beam

Vlaho Žuvelek[1], Ivan Ćurković[2], Ivan Lukačević[3], Andrea Rajić[4]

Abstract

Nowadays, composite steel-concrete systems are among the most cost-effective construction systems for application in multi-storey buildings as they combine structural efficiency and allow accelerated construction speed. Additional optimisation of these systems is possible through the application of cold-formed steel elements and innovative solutions for shear connections. Such optimisation of composite systems is the topic of the LWT-FLOOR project ongoing at the Faculty of Civil Engineering in Zagreb. This paper presents a numerical study of two various cold-formed steel beam types connected to a concrete slab placed within profiled steel sheeting and interconnected using the bolted shear connection. The first cold-formed steel beam type consists of built-up sections using back-to-back cold-formed steel C profiles, while the second type additionally uses a corrugated web inserted between the webs of the cold-formed steel C profiles. To evaluate shear connection behaviour, simulations of the push-out test are performed where either solution with two bolts per rib placed symmetrically or the solution with one bolt per rib placed in a staggered manner is used. Compared to the shear connection with two bolts per rib it is expected that staggered bolt placement would have much less influence on the shear connection strength in the case of cold-formed steel profiles without corrugated web than in the case when the corrugated web is used. Furthermore, a previous study on the behaviour of bolted shear connection in composite systems using cold-formed steel profiles indicates that the proposed values of the reduction factor, k_t when profiled steel sheeting ribs are placed transverse to the steel beam may be too conservative or, in some cases, even completely unnecessary. Therefore, a numerical study on the composite system using cold-formed steel profiles and the corrugated web was further expanded to evaluate the influence of different parameters on the value of the reduction factor.

1. Introduction

Nowadays, topics about the impact of the built environment on the entire ecosystem have become widely researched. Such topics deal with the sustainability of the construction industry, which is achievable by increasing the values of building components and materials during their entire life cycle. An excellent example of such an approach are composite steel-concrete structural systems, which are one of the most cost-effective in the construction industry. They ensure a high level of construction efficiency and, at the same time, enable shorter construction times. The structural efficiency of the system is directly related to the efficiency of individual elements of which the system is composed, which is achieved through partial or complete avoidance of their inherent disadvantages. The advantages of composite steel-concrete structural systems can be further improved by using the newly proposed structural system, which contains built-up innovative cold-formed steel girders with a corrugated web and concrete slabs connected using demountable bolted shear connections. The application of CFS sections in steel-concrete composite floor systems can result in many advantages depending on the applied structural solutions [1–4]. For instance, compared to hot-rolled or welded I-section, applying a corrugated web weight can be significantly reduced while local and global stabilities are increased.

One of the purposes of this paper is to present the scientific project LWT-FLOOR, which is ongoing at the University of Zagreb, Faculty of Civil Engineering, Croatia. The purpose of the project is to investigate the behaviour of the newly proposed structural system which is comprised of built-up CFS with corrugated web connected by spot welds and concrete slab with an innovative type of shear connection. Also, the goal of the project is to investigate all the components of the proposed system using numerical, experimental and probabilistic methods, as well as ultimately establish analytical proposals for the design recommendations.

[1] Research Assistant, Structural Engineering Department, Faculty of Civil Engineering, University of Zagreb, vlaho.zuvelek@grad.unizg.hr
[2] Assistant Professor, Structural Engineering Department, Faculty of Civil Engineering, University of Zagreb, ivan.curkovic@grad.unizg.hr
[3] Assistant Professor, Structural Engineering Department, Faculty of Civil Engineering, University of Zagreb, ivan.lukacevic@grad.unizg.hr
[4] Research Assistant, Structural Engineering Department, Faculty of Civil Engineering, University of Zagreb, andrea.rajic@grad.unizg.hr

This paper aims to present the results of a numerical investigation of a demountable bolted shear connection that is suitable for two proposed composite systems. Also, the paper presents the influence of different effects on the behaviour of the composite system, such as bolt diameter, the position of the bolts in the rib of the concrete slab and the application of different types of the profiled steel sheeting (PSS).

2. Review of previous research

Research shows that composite systems made of cold-formed steel and concrete achieve additional advantages over traditional solutions. Application of CFS profiles alone in composite steel-concrete floor systems can result in many benefits such as reduction of the overall slab depth, freedom in cross-section design, ease of adaptation to irregular floor layouts, fast and wide product availability everywhere as a consequence of simple manufacturing technology, the flexibility of section assembly either in the workshop or on-site [5]. However, CFS profiles have certain disadvantages or limitations when larger spans need to be covered. Such a problem is manifested due to the slenderness of the CFS cross-section, which is why larger cross-sections are required when bridging larger spans. This can be avoided by using corrugated web beams. The use of corrugated web enables the application of thinner sheets in composite structural systems that do not require additional stiffening, which ultimately results in cost savings compared to conventionally made steel profiles and standard hot-rolled beams of 10-30%, or more than 30%. For example, a sinusoidal corrugated web plate with a thickness of 1 mm has a buckling resistance equal to a flat plate with a thickness of at least 12 mm [6]. Corrugated web beam solutions usually use flat plates as flanges that require specific welding technology to be welded to the corrugated web and, as such, have many difficulties [7]. Instead, the use of CFS profiles was proposed, allowing the use of various more simple connection methods, such as screws, spot-welds or cold metal transfer techniques, all of which have been readily investigated [8–10], proving that spot-welds provide the most desirable behaviour. Using the spot-welding technique to connect corrugated web with CFS profiles results in excellent ductility and load-bearing capacity. Therefore, spot-welded beams possess higher stiffness and load-bearing capacity instead of beams that use self-drilling screws as a method of connection [11,12]. Also, using spot welding enables standardisation of detailing in design and fabrication and allows automatization of the production process, which ultimately results in faster production of built-up CFS profiles with corrugated webs [13].

An important segment of the structural behaviour of composite steel-concrete beams is the shear connection, which enables the interaction of individual system components. The behaviour of the shear connection alone is dependent on its strength, i.e., the degree of shear connection, which can be defined as the ratio of shear capacity provided by the interconnecting elements over the capacity of the composite cross-section weakest component (in this case CFS beam or concrete slab). Welded headed studs are the most common type of shear connection in composite steel-concrete beams, as well as the only shear connection standardised by Eurocode [14]. Given today's sustainability approach in of construction industry, the performance of the composite system with a demountable bolted shear connection represents an extremely interesting construction solution. This type of bolt allows easy disassembly of the concrete plate in the case of renovation or modernisation, which is impossible with traditional bolts. Examples of such solutions are given in Figure 1 [15].

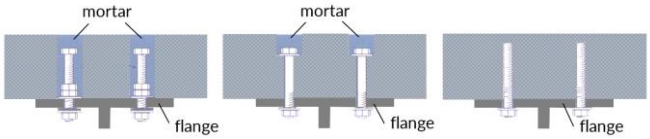

Figure 1: Examples of demountable shear connections

A detailed chronological overview of the shear connections enabling the disassembly of the coupled system components was recently presented in the paper by Jakovljević et al. [16]. The authors indicate that there are major problems related to the resistance and ductility of various demountable shear connections, which require further research. Among the first studies on the behaviour of shear connection between CFS profile and concrete slabs was the one by Hanaor [5], where two types of connection, embedded and dry, were considered. The embedded solution consists of channel sections that are connected in two ways with the beam section, by welding or using 6 mm diameter screws. Based on the obtained results, it can be concluded that this type of shear connection results in a higher capacity than the capacity computed according to the standards regarding fasteners in the CFS section, proving that the appropriate code provisions can be used when adequate test data is unavailable. Hosseinpour et al. [17] present an experimental investigation of bolted shear connectors in the composite CFS beams as a suitable alternative to welded shear studs. The behaviour of the shear connection was observed when certain parameters, such as CFS thickness, size and strength of the bolts, were varied. From the obtained results, models with thinner CFS profiles show a slight elongation of the bolt hole, which is accompanied by buckling of the CFS beam's flanges. On the other hand, in models with thicker CFS profiles, in addition to small elongation of a bolt hole in CFS profiles, yielding of bolts as cracking of concrete slabs and shear of bolts could be also observed as accompanying failure modes. Lakkavalli and You [18] conducted a series of push-out tests where they studied four shear transfer mechanism types, namely surface bonds, prefabricated bent-up tabs, pre-

drilled holes, and screws, in order to srealise the connection between CFS C sections with concrete slabs. Hsu et al. [4] researched a newly proposed system containing a reinforced concrete slab on a corrugated metal deck, back-to-back cold-formed steel joists, and a continuous cold-formed furring shear connector. The test results show that the composite sections could reach ultimate strength without local shear or buckling failure. Irwan et al. [3] conducted experiments on an innovative shear connection solution using bent-up triangular tabs. Based on the conducted tests, it could be observed that the main failure modes are concrete crushing and splitting, and the slip itself is less than the limit value of 6 mm according to Eurocode 4 [14]. The authors also concluded that the shear resistance of the joint could be increased by increasing either the CFS thickness, the tab angle or its size. An additional contribution was made by establishing an resistance model or the design of such a shear connection that correlates with test results. However, further testing is required to confirm this. Alhajri et al. [19] conducted an experimental study on the behaviour of composite beams containing CFS sections and ferro-cement slabs connected using 12 mm diameter bolts as shear connectors. Bamaga et al. [20] recently proposed three solutions of demountable shear connection using either hot-rolled steel plate, single-bracket or double-bracket as shear connectors. They conducted a series of push-out tests of the proposed solutions, from which it was possible to conclude that all three solutions achieve adequate strength capacity as well as ductility.

All of the above indicates that the behaviour of CFS in composite structure has not yet been sufficiently investigated, as well as the effect of the shear connection itself, and further research is needed. Therefore, the research project LWT-FLOOR was established, where one of the aims is to contribute to greater knowledge regarding the behaviour of shear connection in CFS-concrete composite structural systems.

3. Finite element model

3.1 Geometry and finite element modelling

In this study, Abaqus software was used to develop three-dimensional push-out test models. In order to encompass geometrical and material nonlinearities, analysis was performed using the ABAQUS Explicit solver [21]. As previously mentioned, a numerical investigation of the demountable bolted shear connection in composite CFS-concrete systems was carried out. Two systems of composite structures were observed where the first system consists of a built-up CFS beam with a corrugated web connected using spot-welding technology and a concrete slab connected using shear connectors, Figure 2 (a), while the second system consists of back-to-back CFS beam assembled with the help of spot-welds and a concrete slab that is also connected using shear connectors, Figure 2. (b). For further reference, MW and S models are systems that contain a corrugated web, while M models are without a corrugated web. The experimental push-out specimen consists of two concrete slabs which are connected to a CFS beam using a bolted shear connection. Therefore, due to the symmetry of the test specimen, half of the model is modelled in this work, which shortens the needed computational time. The demountable shear connection was achieved using bolts as shear connectors with embedded nuts in concrete slabs (single-nut has been embedded on the concrete side). Using such bolts makes it possible to control bolt rotation and slip during loading [16]. The bolts are installed through pre-drilled holes in the ribs of PSS and CFS profiles in experimental testing. In this study, bolts of a diameter of 12 mm and 16 mm were used, which corresponds to the bolts that will be used in the experiment. To achieve the most accurate behaviour of the bolts, a reduced diameter was adopted within the models in the area of the bolt threads. The reduced diameter is only adopted between the two nuts because outside this area, it will not affect the behaviour of the model. The bolt diameter at the thread is calculated from the net surface of the bolt core within this area [22], where the obtained values are 10.4 mm and 14.1 mm for M12 and M16, respectively. The M16 bolts were used to fulfil the conditions of the minimum value of the diameter of headed studs as given in EN 1994-1-1 [14]. Meanwhile, M12 bolts are used as structural bolts with a minimum diameter according to EN 1090-2 [23]. All bolts in the models are of grade 8.8, which is one of the most commonly used grades for structural bolts. With this type of shear connection, due to the geometry of the concrete and the profiled sheet, it is necessary to meet the minimum height of the bolt in the concrete slab prescribed by EN 1994-1-1 [14]. Therefore, in the M and MW models, the height of the bolt within the concrete is 95 mm, while in the S models, it is 120 mm. As previously mentioned, in each system, two bolt positions were observed, in pairs and staggered positions, Figure 2 (c). Also, in this study, a numerical investigation of the effect of the different types of PSS (open or re-entrant trough profile) on the final behaviour of the system with the corrugated web was carried out, Figure 3.

Table 1 shows 24 different models that were considered within this study. Here, variations such as the diameter of the bolts, the position of the bolts, and the type and geometry of the PSS have been made. The nominal geometry of the components is adopted according to the geometry that will be used in the upcoming experimental testing. Therefore, CFS C profiles have dimensions of 120x47x3 mm, corrugated web 780x120x1.25, PSS 720x600 with a thickness of 1 mm and concrete slab 720x600x140 mm. The concrete slab is reinforced with Q524 reinforcing mesh, where 10 mm diameter bars are spaced 150 mm apart in each direction.

The main parts of the model were modelled as 3-D deformable solid elements (C3D8R), such as concrete slabs, CFS C-profiles and bolts. Due to an insignificant ratio of thickness to length or width, shell elements (S4R) were used for corrugated web and PSS, while wire elements (T3D2) were adopted for reinforcement mesh.

Table 1: Specification of investigated numerical models

Model name	Bolts	Bolt position	Profiled steel sheeting [mm] h_p	Profiled steel sheeting [mm] b_o	Concrete class	Corrugated web	Type of PSS
M1W_1	M12	Pairs	60	120	C20/25	✓	open trough profile
M1W_2		Staggered				✓	
M1_1		Pairs				✕	
M1_2		Staggered				✕	
M2W_1	M16	Pairs				✓	
M2W_2		Staggered				✓	
M2_1		Pairs				✕	
M2_2		Staggered				✕	
S1_1	M12	Pairs	60	95		✓	open trough profile
S1_2			60	120			
S1_3			85	90			
S1_4			85	120			
S2_1	M16		60	95			
S2_2			60	120			
S2_3			85	90			
S2_4			85	120			
S3_1	M12		60	95			re-entrant trough profile
S3_2			60	120			
S3_3			85	90			
S3_4			85	120			
S4_1	M16		60	95			
S4_2			60	120			
S4_3			85	90			
S4_4			85	120			

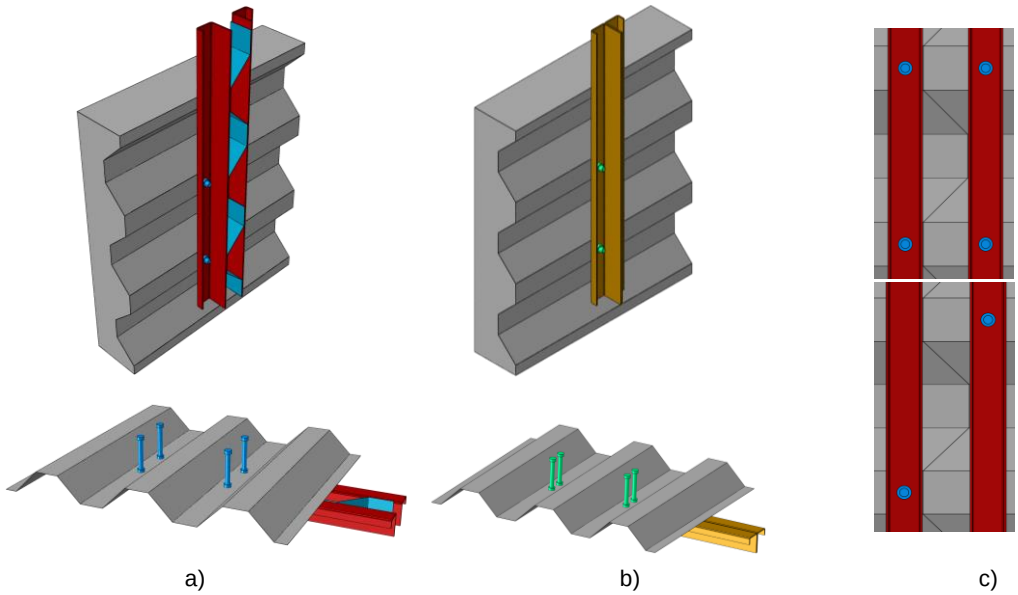

a) b) c)

Figure 2: Finite element models of specimens with bolted shear connection: a) with corrugated web (MW and S models); b) without corrugated web (M models); c) position of bolts (pairs and staggered)

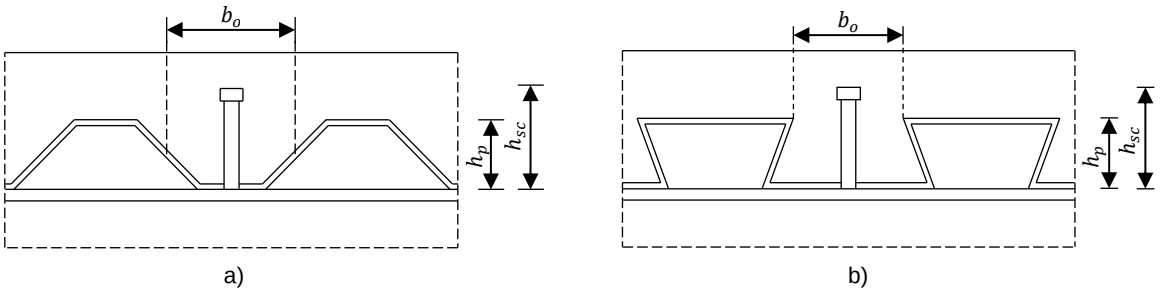

a) b)

Figure 3: The cross-sections of PSS: a) open through profile for S1 and S2 models; b) re-entrant through profile for S3 and S4 models

3.2 Material properties

3.2.1 Steel

A bilinear stress-strain curve is adopted in Abaqus to represent the behaviour of steel according to EN 1993-1-5 Annex C [24]. For all steel elements in the models, the modulus of the elasticity, the Poisson ratio, and the density values were taken as 210 GPa, 0.3 and 7850 kg/m^3, respectively. As previously mentioned, cold-formed steel S350GD was used in the models, whose yield and ultimate stresses were considered to be 350 MPa and 420 MPa, respectively. For bolt grade 8.8, the yield and ultimate stress values of 640 MPa and 800 MPa were used, respectively. In addition to stresses, it is necessary to define the ultimate strain, ε_{us}, which for steel S350GD is adopted as 15%, while for bolts as 12%. The material for reinforcing mesh was defined, so that yield and ultimate stresses were taken as equal, corresponding to the value of 500 MPa.

3.2.2 Concrete

In order to simulate the behaviour of the reinforced concrete slab as accurately as possible, the concrete damaged plasticity model (CDP) was adopted in the models. This model is primarily based on defining the compressive and tensile behaviour of concrete, i.e. defining the two main failure modes, crushing in compression and cracking in tension. The CDP model was developed in accordance with papers [25,26] using the material characteristics of the applied concrete class in accordance with EN 1992-1-1 [27]. The values of the parameters for the CDP model used in this paper are shown in Table 2.

Table 2: Plastic parameters for CDP model of concrete slab

Dilation angle	Eccentricity	F_{b0}/F_{c0}	K	Viscosity Parameter
31	0.1	1.16	0.667	0.001

The stiffness degradation d_c due to concrete crushing was calculated as:

$$d_c = 1 - \frac{\sigma_c}{f_{cm}} \quad (1)$$

The compressive stress-strain curve of the concrete according to the EN 1992-1-1 [27] with stiffness degradation of concrete is presented in Figure 4. Figure 5 represents an extension of the Eurocode compressive stress-strain relationship model based on research by Pavlović et al. [28]. Such a model was used here because it considers the overall crushing strength of concrete.

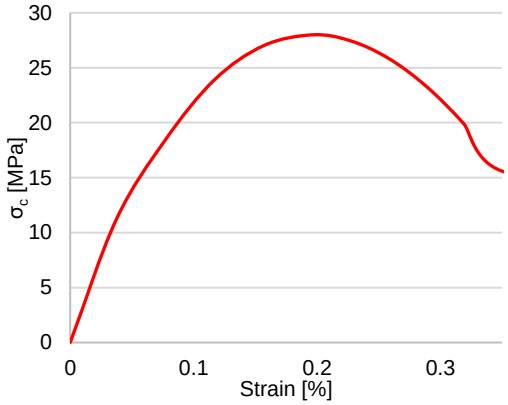

Figure 4: Stress-strain curve for concrete according to EN 1992-1-1

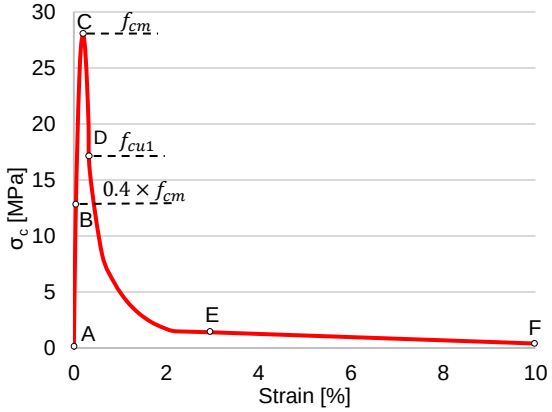

Figure 5: Parameters of concrete behaviour in compression, an extension of EN 1992-1-1 model

The tensile behaviour of concrete is defined by the tension plasticity curve, which is defined as a function of cracking

displacement and tensile stress. Tensile behaviour is defined by an exponential function given by [29]:

$$\frac{\sigma}{f_t} = f(w) - \frac{w}{w_c} f(w_c) \quad (2)$$

$$f(w) = \left[1 + \left(\frac{c_1 w}{w_c}\right)^3\right] \exp\left(-\frac{c_2 w}{w_c}\right) \quad (3)$$

where w is the crack opening displacement, while w_c is the critical crack opening displacement at which stress can no longer be transferred.

According to Cornelissen et al. [29], the value of the critical crack opening displacement, w_c, can be calculated

$$w_c = \frac{5.14 \cdot G_f}{f_t} \quad (4)$$

where, c_1 and c_2 are material constants. For normal density concrete c_1 and c_2 values are 3.0 and 6.93, respectively.

G_f represents fracture energy, i.e. the energy required for the development of the unit area of the crack, which is calculated according to the expression proposed by [25,30]:

$$G_f = 73 \cdot {f_{cm}}^{0.18} \quad (5)$$

The value of stiffness degradation in tension d_t can be calculated as:

$$d_t = 1 - \frac{\sigma_t}{f_t} \quad (6)$$

Based on all these expressions, the tensile behaviour of concrete is shown in Figures 6 a) and b).

To calculate all the necessary parameters, the concrete density of 2400 kg/m^3 was adopted in the models.

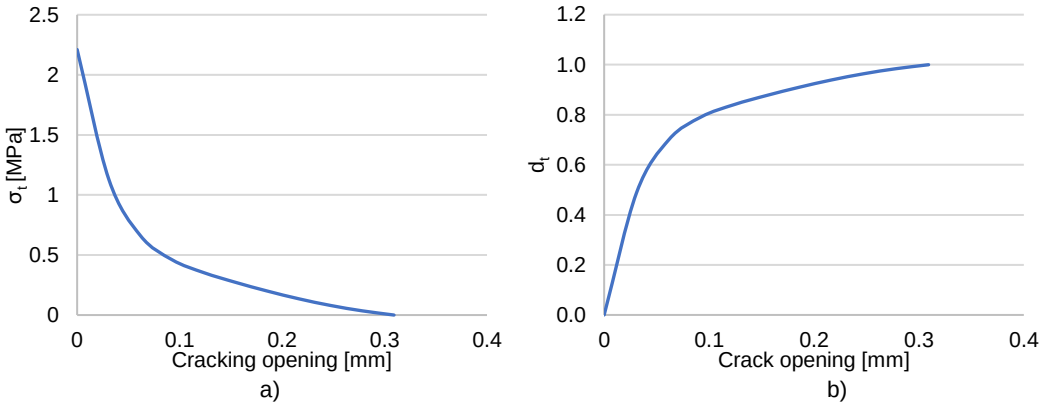

Figure 6: Parameters of concrete in tension: a) tensile stress versus cracking displacement; b) tensile damage versus cracking displacement

3.3 Boundary and Load Conditions

In this study, symmetric boundary conditions were applied to the plane orthogonal to the X-axis, which prevents displacement in the X direction as well as rotations around the Y and Z axes. Since the concrete slab rests on the fixed stand on the bottom sides, those are then fixed using fully rigid boundary conditions. This ensures that the concrete slab does not move due to the translation of the CFS beam. Also, at the top of the CFS beam, where displacement input is realised, rotations and displacements in the horizontal X and Z directions were prevented to avoid unwanted behaviour.

As previously mentioned, the Abaqus Explicit solver was applied due to many elements and contact and the nonlinear behaviour of the material. For such a solver to be used, it is necessary to satisfy the condition that the kinetic energy of the model should not exceed 10% of the total internal energy. Based on this statement, an analysis was made where kinetic energy was compared with total internal energy, after which the results showed that this type of solver could be used. Therefore, in the models, a uniform vertical displacement (Y-axis) was applied at the top of the CFS beam, with a value of 10 mm per second, using the displacement control method.

3.4 Interaction properties

In order to enable the interaction of different elements in FE models, it is necessary to define the contact conditions between the modelled elements. In this paper, contacts are defined to apply vertical and horizontal interaction forces between surfaces properly. Contact properties are defined through the normal and tangential behaviour of the contact surface. In normal behaviour, Hard Contact is defined, which minimises the penetration of the slave surface into the master surface. Tangential behaviour was simulated by the

penalty friction method [21]. For friction coefficient value of 0.3 was assumed for all interactions, which is in the range of the values proposed by [26,31]. Reinforcement mesh was embedded in the concrete slab, which led to neglection of relative slip as well as debonding of the reinforcement from concrete.

As previously mentioned, the reduction of bolt cross-section due to thread existence is considered. However, the influence of nut tightening on the bolt is not considered, i.e. the bolt and nut are modelled as one single element. CFS beams are assembled using spot welds which are modelled as rigid points using MPC Link constraint to avoid failure. Table 3 shows all the interactions considered in the FE model.

Table 3: Interactions definition between the elements of the FE model

Name of connection	Type of surface		Contact type
	Master surface	Slave surface	
Bolt - CFS beam	CFS profile	Bolt	Interaction
Nut - CFS beam	CFS profile	Nut	Interaction
Nut - PSS	PSS	Nut	Interaction
Bolt - Concrete slab	Concrete slab	Bolt	Interaction
CFS profile - Corrugated web	CFS profile	Corrugated web	Interaction
CFS profile - PSS	PSS	CFS profile	Interaction
Concrete slab - PSS	Slab PSS	Concrete slab	Interaction
Spot welds	-	-	Constraint (MPC Link)
Concrete slab - reinforcement	-	-	Embedded

4. Results and discussion

Four failure modes, shown in Figure 7, can be observed based on the obtained results. The first failure mode is a concrete failure, where concrete crushing and the formation of cracks around the shear connector were observed, which is also the most common mode of failure in composite structures. The second failure mode is related to reaching the bearing resistance of the bolt hole in the CFS profile. In some models, a small elongation of the bolt hole was observed, which was accompanied by an inclination of the nut through the stretched holes. The third failure mode is manifested as the combination of two failure modes, concrete crushing and stability loss. Such a failure mode occurs due to rib failure in models containing re-entrant through PSS from Figure 3 (b), whose failure ultimately results in the loss of stability of the CFS profile. The fourth failure mode is the yielding of bolted shear connectors in shear, i.e. shear failure at the area of the bolt thread.

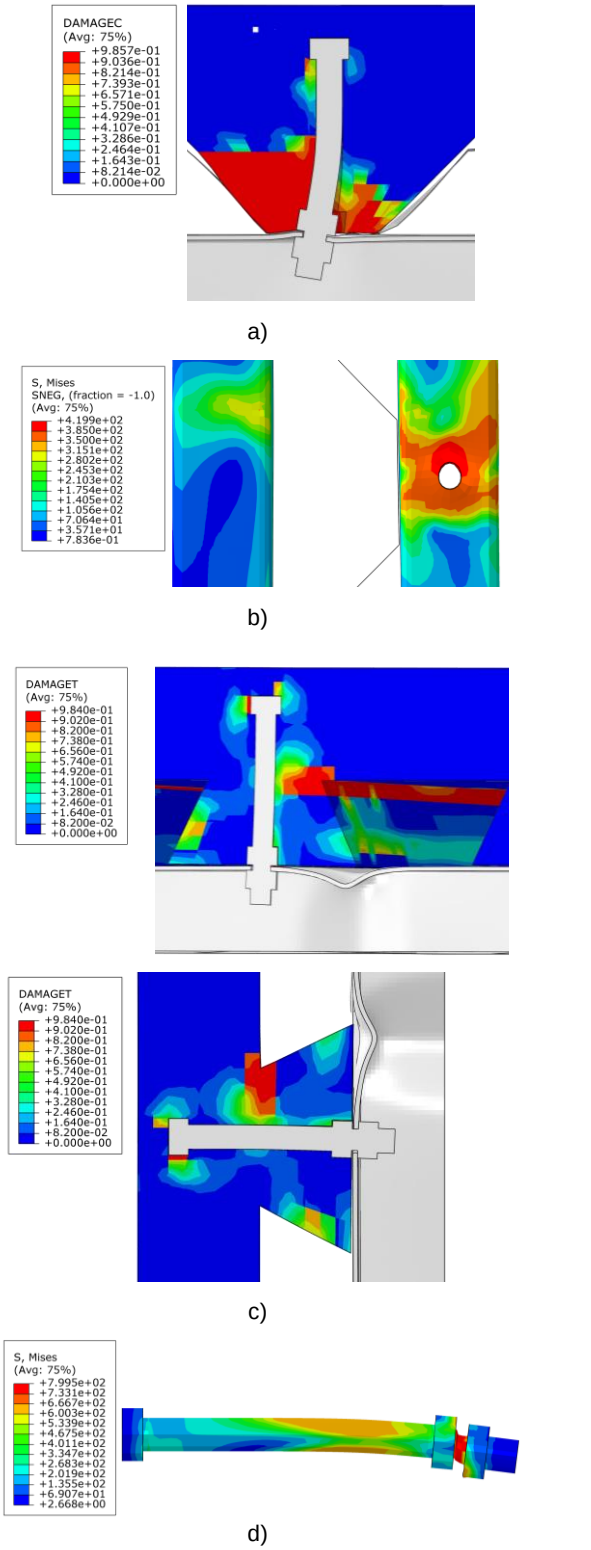

Figure 7: Main failure modes: a) concrete failure (compressive damage); b) bearing resistance of the bolt hole; c) concrete failure (tensile damage) and stability loss; d) shear failure of bolts

4.1 Effect of variation of connector placement

In this section, the M and MW models were analysed, which contain either two bolts per rib or one bolt per rib placed in a staggered position, Figure 2 (c). The results obtained from the numerical analysis were compared to the characteristic values that can be calculated using Eurocodes, either EN 1993-1-8 [32] or EN 1994-1-1 [14]. The calculated characteristic values included CFS profile hole bearing resistance ($F_{b,Rk}$), CFS profile cross-section resistance (N_{Rk}), and shear resistance of one connector due to steel failure ($P_{Rk,S}$) or due to concrete failure ($P_{Rk,C}$) with and without reduction factor due to the transverse placement of the PSS ribs, k_t. The reduction factor, k_t, is calculated in accordance with EN 1994-1-1 [14] as:

$$k_t = \frac{0.7}{\sqrt{n_r}} \frac{b_o}{h_p} \left(\frac{h_{sc}}{h_p} - 1 \right) \quad (7)$$

where n_r is the number of stud connectors per rib, while the other values are as defined in Figure 3. For the chosen geometry of the PSS, the calculated reduction factor for models containing two bolts per rib is 0.58, while for models with one bolt per rib placed in a staggered manner is 0.81. Table 4 presents characteristic resistances of individual components according to Eurocodes for various analysed numerical models.

Table 4: Characteristic resistances of individual components in [kN] according to Eurocode for various models

Model name	$F_{b,Rk}$	N_{Rk}	$P_{Rk,S}$	$k_t \cdot P_{Rk,S}$	$P_{Rk,C}$	$k_t \cdot P_{Rk,C}$
M1W_1	32.8	235	54.4	31.6	32.3	18.7
M1W_2				44.1		26.2
M1_1				31.6		18.7
M1_2				44.1		26.2
M2W_1	44.4	235	100	58	57.5	33.4
M2W_2				81		46.6
M2_1				58		33.4
M2_2				81		46.6

In order for the characteristic values from Table 4, to be comparable with the numerical values, it is necessary to multiply them by eight for models that contain two bolts per rib or by four for models that contain one bolt per rib placed in a staggered position, except for the N_{Rk} value which must be multiplied by 2. A comparison of analytical and numerical values is given in Table 5.

From the obtained force-displacement curves, Figure 8, for the models with two bolts per rib, it can be observed that models with a corrugated web (M1W_1 and M2W_1) achieve greater resistance compared to models without a corrugated web (M1_1 and M2_1). Such behaviour of the model without a corrugated web can be explained by the fact due to the small spacing of the shear connectors. In that case, achievement of the full concrete bearing capacity of the shear connector is precluded as the failure areas of each connector overlap very soon. However, the models containing one bolt per rib in the staggered position, either with a corrugated web (M1W_2 and M2W_2) or without it (M1_2 and M2_2), achieve similar resistance and ductility. Such behaviour occurred due to the increased distance between the bolts, which prevented early overlap of concrete failure areas and allowed for the development of the full bearing capacity of shear connectors in concrete.

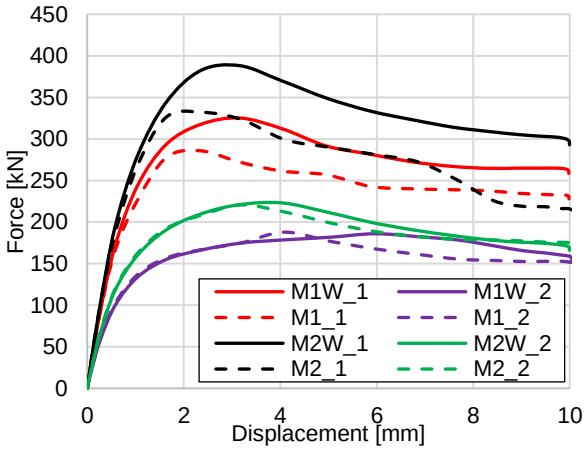

Figure 8: Force-displacement curves for M and MW models

Table 5: Comparison of numerical and analytically calculated values for selected failure mode in [kN]

Model name	F_{NUM}	Failure mode	F_{CALC}	$\frac{F_{CALC}}{F_{NUM}}$	$k_t \cdot F_{CALC}$	$\frac{k_t \cdot F_{CALC}}{F_{NUM}}$
M1W_1	324	Concrete	258	0.80	149.6	0.46
M1W_2	186	Concrete	129	0.70	105	0.56
M1_1	286	Concrete	258	0.90	149.6	0.52
M1_2	188	Concrete	129	0.70	105	0.56
M2W_1	388	Concrete	460	1.19	268	0.70
M2W_2	224	Concrete	230	1.03	186	0.83
M2_1	332	Concrete	460	1.39	268	0.81
M2_2	220	Concrete	230	1.05	186	0.85

Based on the comparison from Table 5, it can be seen that the reduction factor, k_t, for bolts of smaller diameter can be ignored, or modified values can be used, while for M16 bolts, it must be taken into account. However, it should be noted that the reduction factor values given according to EN 1994-1-1 [14] are still too conservative. Although, the application of the reduction factor, calculated according to EN 1994-1-1 [14], is questionable, considering that the material and diameter constraints for its application are not met within this research.

4.2 Effects of variation of PSS type

In this section, models with different types of the profiled steel sheet are considered, i.e. models S1 and S2 contain open trough PSS, Figure 3 (a), while S3 and S4 contain re-entrant trough PSS, Figure 3 (b). The geometry of the PSS is given in Table 1.

Table 6: Characteristic resistances of individual components in kN according to Eurocode for various models

Model name	$F_{b,Rk}$	$F_{v,Rk}$	N_{Rk}	$P_{Rk,S}$	$P_{Rk,C}$	k_t	k_{t,up_limits}	$k_t \cdot P_{Rk,S}$	$k_t \cdot P_{Rk,C}$
S1_1	32.8	162	235	54.4	32.3	0.74	0.70	38.1	22.61
S1_2	32.8	162	235	54.4	32.3	0.99	0.70	38.1	22.61
S1_3	32.8	162	235	54.4	32.3	0.22		12	7.11
S1_4	32.8	162	235	54.4	32.3	0.29		15.81	9.37
S2_1	44.4	302	235	100	57.5	0.74	0.70	70	40.25
S2_2	44.4	302	235	100	57.5	0.99	0.70	70	40.25
S2_3	44.4	302	235	100	57.5	0.22		22	12.65
S2_4	44.4	302	235	100	57.5	0.29		29	16.68
S3_1	32.8	162	235	54.4	32.3	0.74	0.70	38.1	22.61
S3_2	32.8	162	235	54.4	32.3	0.99	0.70	38.1	22.61
S3_3	32.8	162	235	54.4	32.3	0.22		12	7.11
S3_4	32.8	162	235	54.4	32.3	0.29		15.81	9.37
S4_1	44.4	302	235	100	57.5	0.74	0.70	70	40.25
S4_2	44.4	302	235	100	57.5	0.99	0.70	70	40.25
S4_3	44.4	302	235	100	57.5	0.22		22	12.65
S4_4	44.4	302	235	100	57.5	0.29		29	16.68

Using the different geometry of the PSS requires the calculation of the reduction factor for each model. Therefore, Table 6 presents the calculated characteristic values as well as the values of the reduction factor, k_t, and its upper limit values, k_{t,up_limits}.

In order for the values from Table 6 to be comparable with the numerical values, it is necessary to multiply them by eight because the analysed models contain four studs, except for N_{Rk} which must be multiplied by two.

The numerically obtained relation between force and displacement for models S1 and S2 are presented in Figure 9. Based on the shape of the curves for the S1 and S2 models, the same mode of failure can be observed, i.e., concrete failure. It can be seen that changing the PSS geometry affects the resistance and behaviour of the model. Therefore, by increasing the height of the rib h_p, a lower resistance of the model is obtained. In other words, models with a greater PSS rib height of (S1_3, S1_4, S2_3 and S2_4) achieve lower resistance due to the reduction of the concrete slab thickness above the. However, in models (S1_2, S1_4, S2_2 and S2_4) that contain wider PSS ribs (larger b_o values), compared to other models, a higher resistance of shear connectors in concrete is achieved, which is expected considering that the volume of the concrete, with such geometry, increases. However, models (S1_1, S1_3, S2_1 and S2_3) with narrower PSS ribs (smaller b_o values) achieved slightly better performance in terms of ductility. It can also be seen that increasing the diameter of the bolts (S2 models) increases the bearing capacity and stiffness.

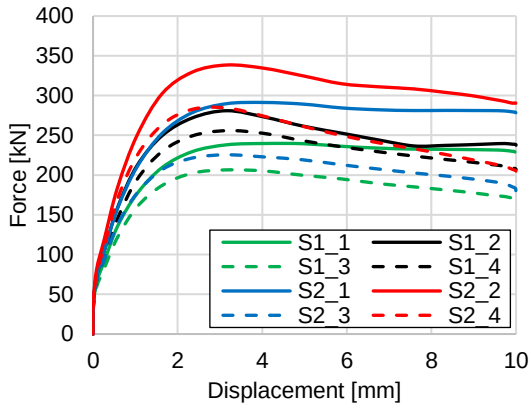

Figure 9. Force-displacement curves for models S1 and S2

From Figure 10, it is possible to observe all types of failure modes in models S3 and S4 based on the different shapes of the curves. By investigating some S3 models (S3_1 and S3_2), it can be seen that the bolt holes have reached their bearing resistance, and their elongation has occurred. Further stress development leads to shear failure in the threaded area of the bolt. The curves of models S3_3 and S3_4 indicate that concrete failure occurred due to the formation of a tensile crack. The analogy of the influence of the PSS geometry on the behaviour of the model is similar

to the previously mentioned S1 and S2 models. However, although Table 6 indicates that the failure of the shear connector in concrete should primarily occur, the numerically obtained turns out to be higher, which leads to bolt shear failure within the threaded area (S3_1 and S3_2 models). The S3_3 and S3_4 models contain a higher rib height, which results in reduced shear resistance compared to S3_1 and S3_2 models and ultimately leads to a different failure mode, i.e. cracking of concrete.

Investigating S4 models, one can observe that a combined failure mode occurred in some models (S4_1 and S4_2). Initially, concrete failure occurs due to the formation of tensile cracks shown in Figure 7 (c), which leads to the breaking of the concrete slab rib and ultimately results in the loss of stability of the CFS C profile. In other S4 models (S4_3 and S4_4), pure concrete failure mode has occurred. Also, from the curves of the S4 models, Figure 11, the effect of varying PSS geometry on the overall resistance of the model is visible. It can be seen that even in these models, increasing the diameter of the bolt leads to an increase in stiffness and bearing resistance.

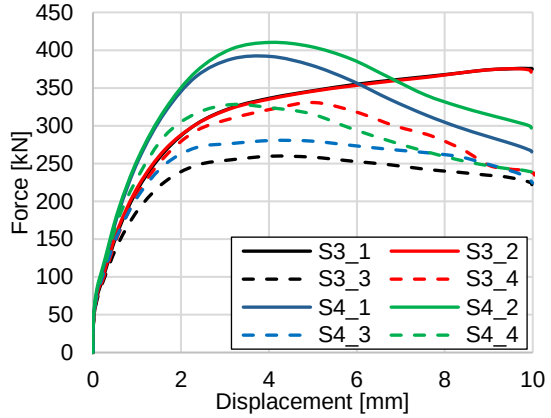

Figure 10: Force-displacement curves for models S3/S4

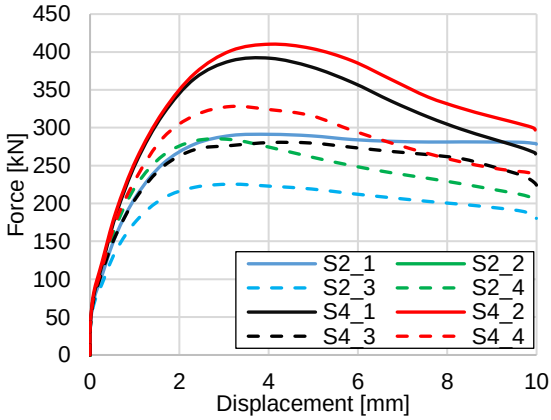

Figure 11. Force-displacement curves for models S2/S4

Figure 11 shows the curves of S2 and S4 models containing different types of PSS. By comparing the obtained curves, it can be concluded that the S4 models containing the PSS with re-entrant troughs achieve greater resistance with similar stiffness and ductility compared to the S2 models. However, the reduction factor values for S2 and S4 models are the same because the same equation, Eq. (12), covers both PSS.

Table 7: Comparison of numerical and analytically calculated values for selected models in [kN]

Model name	F_{NUM}	Failure mode	F_{CALC}	$\frac{F_{CALC}}{F_{NUM}}$	$k_t \cdot F_{CALC}$	$\frac{k_t \cdot F_{CALC}}{F_{NUM}}$
S1_1	240	C.C.	258	1.07	181	0.75
S1_2	281	C.C.	258	0.92	181	0.64
S1_3	207	C.C.	258	1.24	56.8	0.27
S1_4	256	C.C.	258	1.01	74.8	0.29
S2_1	293	C.C.	460	1.57	322	1.09
S2_2	339	C.C.	460	1.35	322	0.95
S2_3	226	C.C.	460	2.04	102	0.38
S2_4	285	C.C.	460	1.61	133	0.46
S3_1	376	S.B.	324	0.86	-	-
S3_2	376	S.B.	324	0.86	-	-
S3_3	260	C.C.	258	0.99	56.8	0.22
S3_4	332	C.C.	258	0.78	74.8	0.23
S4_1	392	C.C/S.	460	1.18	322	0.82
S4_2	411	C.C/S.	460	1.12	322	0.78
S4_3	281	C.C.	460	1.63	102	0.36
S4_4	328	C.C.	460	1.40	133	0.41

Note: C.C.= concrete slab cracking; S.B.= Bolt shear failure; S.= CFS C profile stability loss

As previously mentioned, the obtained results indicate that the reduction factor can be neglected or should use modified values for M12 bolts, while for M16 bolts, it should be taken into account. However, it is still evident that the reduction factor values given in EN 1994-1-1 [14] are too conservative considering the changing values of the parameters that affect its value according to Eq. (12). It is also worth noting that lower values of the reduction factor result in a significant reduction of the characteristic values, which ultimately significantly deviates from the numerical values. Based on this, it can be assumed that in the future, some lower limits can also be proposed for the reduction factor, as there are currently only upper limits provided.

5. Conclusions

In this study, 24 model push-out tests were simulated to expand the knowledge about the behaviour of CFS in composite structures. Also, the simulation of these models laid the foundation for future experimental tests. The obtained results provide the following conclusions, which need further confirmation from the experimental tests:

- Placing two shear connectors per rib at a relatively small distance, as is the case in back-to-back systems, causes an overlap of the concrete failure area at the early loading stage. Placing one

connector per rib in a staggered manner allowed the development of the full bearing capacity of the concrete in the profiled steel sheeting.

- The influence of the bolt diameter on concrete failure when the ribs of the PSS are transverse to the beam should be investigated in more detail. The obtained numerical results indicate that the reduction factor might be increased, and even, for smaller bolt diameters, it could be omitted entirely.
- In addition, the validation of the use of the reduction factor should be checked experimentally if shear connectors with a diameter of less than 16 mm and a quality greater than 450 N/mm^2 are used.
- Changing the type of PSS from the one with open troughs to the one with re-entrant troughs resulted in greater resistance with similar stiffness and ductility.
- Changing the geometry of the PSS results in different failure modes, which need to be taken into account.

6. Acknowledgments

This work has been supported in part by Croatian Science Foundation under the project UIP-2020-02-2964.

References

[1] Wehbe, N.; Bahmani, P.; Wehbe, A. Behavior of Concrete/Cold Formed Steel Composite Beams: Experimental Development of a Novel Structural System. Int. J. Concr. Struct. Mater. 2013, 7, 51–59, doi:10.1007/s40069-013-0031-6.

[2] Bamaga, S.O.; Tahir, M.M.; Tan, T.C.; Mohammad, S.; Yahya, N.; Saleh, A.L.; Mustaffar, M.; Osman, M.H.; Rahman, A.B.A. Feasibility of Developing Composite Action between Concrete and Cold-Formed Steel Beam. J. Cent. South Univ. 2013, 20, 3689–3696, doi:10.1007/s11771-013-1897-9.

[3] M.Irwan, J.; Hanizah, A.H.; Azmi, I. Test of Shear Transfer Enhancement in Symmetric Cold-Formed Steel-Concrete Composite Beams. J. Constr. Steel Res. 2009, 65, 2087–2098, doi:10.1016/j.jcsr.2009.07.008.

[4] Hsu, C.T.T.; Punurai, S.; Punurai, W.; Majdi, Y. New Composite Beams Having Cold-Formed Steel Joists and Concrete Slab. Eng. Struct. 2014, 71, 187–200, doi:10.1016/j.engstruct.2014.04.011.

[5] Hanaor, A. Tests of Composite Beams with Cold-Formed Sections. J. Constr. Steel Res. 2000, 54, 245–264, doi:10.1016/S0143-974X(99)00046-2.

[6] Dubina, D.; Ungureanu, V.; Gîlia, L. Experimental Investigations of Cold-Formed Steel Beams of Corrugated Web and Built-up Section for Flanges. Thin-Walled Struct. 2015, 90, 159–170, doi:10.1016/j.tws.2015.01.018.

[7] Hamada, M.; Nakayama, K.; Kakihara, M.; Saloh, K.; Ohtake, F. Development of Welded I-Beam with Corrugated Web. The Sumitomo Search 1984, 29, 75–90.

[8] Dubina, D.; Ungureanu, V.; Gîlia, L. Cold-Formed Steel Beams with Corrugated Web and Discrete Web-to-Flange Fasteners. Steel Constr. 2013, 6, 74–81, doi:10.1002/stco.201310019.

[9] Ungureanu, V.; Both, I.; Burca, M.; Tunea, D.; Grosan, M.; Neagu, C.; Dubina, D. Welding Technologies for Built-up Cold-Formed Steel Beams: Experimental Investigations. Proc. 9th Int. Conf. Adv. Steel Struct. ICASS 2018 2020, 5–7, doi:10.18057/ICASS2018.P.082.

[10] Benzar, Ş.; Ungureanu, V.; Dubină, D.; Burcă, M. Built-Up Cold-Formed Steel Beams with Corrugated Webs Connected with Spot Welding. Adv. Mater. Res. 2015, 1111, 157–162, doi:10.4028/www.scientific.net/AMR.1111.157.

[11] Neagu, C.; Georgescu, M.; Dubina, D. Experimental Investigations on Built-Up Cold-Formed Steel Beams Using Mig Brazing. 2018.

[12] Ungureanu, V.; Lukačević, I.; Both, I.; Burca, M.; Dubina, D. Built-Up Cold-Formed Steel Beams with Corrugated Webs Connected by Spot Welding - Numerical Investigations. In Proceedings of the International Colloquia on Stability and Ductility of Steel Structures (SDSS 2019); Prague, 2019; p. e-Procedings.

[13] Lukačević, I.; Ćurković, I.; Rajić, A.; Čudina, I. Innovative Lightweight Cold-Formed Steel-Concrete Composite Floor System – LWT-FLOOR Project. IOP Conf. Ser. Mater. Sci. Eng. 2021, 1203, 032078, doi:10.1088/1757-899X/1203/3/032078.

[14] European Commitee for Standardization CEN EN 1994-1-1: Eurocode 4: Design of Composite Steel and Concrete Structures - Part 1-1: General Rules and Rules for Buildings; 2004;

[15] Androić, B.; Dujmović, D.; Lukačević, I. Design of Composite Structures According to Eurocode 4; IA Projektiranje: Zagreb, Croatia: Zagreb, 2012;

[16] Jakovljević, I.; Spremić, M.; Marković, Z. Demountable Composite Steel-Concrete Floors: A State-of-the-Art Review. Gradjevinar 2021, 73, 249–263, doi:10.14256/JCE.2932.2020.

[17] Hosseinpour, M.; Zeynalian, M.; Ataei, A.; Daei, M. Push-out Tests on Bolted Shear Connectors in Composite Cold-Formed Steel Beams. Thin-Walled Struct. 2021, 164, 107831, doi:10.1016/j.tws.2021.107831.

[18] Lakkavalli, B.S.; Liu, Y. Experimental Study of Composite Cold-Formed Steel C-Section Floor Joists. J. Constr. Steel Res. 2006, 62, 995–1006, doi:10.1016/j.jcsr.2006.02.003.

[19] Saggaff, A.; Tahir, M.M.; Azimi, M.; Alhajri, T.M. Structural Aspects of Cold-Formed Steel Section

Designed as U-Shape Composite Beam. AIP Conf. Proc. 2017, 1903, doi:10.1063/1.5011505.
[20] Bamaga, S.O.; Tahir, M.M.; Tan, C.S.; Shek, P.N.; Aghlara, R. Push-out Tests on Three Innovative Shear Connectors for Composite Cold-Formed Steel Concrete Beams. Constr. Build. Mater. 2019, 223, 288–298, doi:10.1016/j.conbuildmat.2019.06.223.
[21] User CAE. Abaqus 2016 2016.
[22] European Commitee for Standardization CEN, EN ISO 898-1: 2013: Mechanical properties of fasteners made of carbon steel and alloy steel – Part 1: Bolts, screws and studs with specified property classes – Coarse thread and fine pitch thread, 2013.
[23] European Commitee for Standardization CEN, EN 1090-2: 2018: Execution of steel structures and aluminium structures – Part 2: Technical requirements for steel structures, 2018.
[24] European Commitee for Standardization CEN, EN 1993-1-5: Eurocode 3: Design of Steel Structures—Part 1-5: Plated Structural Elements,2005.
[25] Lukačević, I.; Ćurković, I.; Rajić, A.; Bartolac, M. Lightweight Composite Floor System—Cold-Formed Steel and Concrete—LWT-FLOOR Project. Buildings 2022, 12, doi:10.3390/buildings12020209.
[26] Arezoomand Langarudi, P.; Ebrahimnejad, M. Numerical Study of the Behavior of Bolted Shear Connectors in Composite Slabs with Steel Deck. Structures 2020, 26, 501–515, doi:10.1016/j.istruc.2020.04.037.
[27] European Commitee for Standardization CEN, EN 1992-1-1: Eurocode 2: Design of Concrete Structures—Part 1-1: General Rules and Rules for Buildings, 2004.
[28] Pavlović, M.; Marković, Z.; Veljković, M.; Bucrossed D Signevac, D. Bolted Shear Connectors vs. Headed Studs Behavior in Push-out Tests. J. Constr. Steel Res. 2013, 88, 134–149, doi:10.1016/j.jcsr.2013.05.003.
[29] Cornelissen, H.A.W.; Hordijk, D.A.; Reinhardt, H.W. Two-Dimensional Theories of Anchorage Zone Stresses in Post-Tensioned Prestressed Beams. ACI J. Proc. 1962, 59, 45–56, doi:10.14359/7961.
[30] Tao, Y.; Chen, J.F. Concrete Damage Plasticity Model for Modeling FRP-to-Concrete Bond Behavior. J. Compos. Constr. 2015, 19, 04014026, doi:10.1061/(asce)cc.1943-5614.0000482.
[31] Patel, V.I.; Uy, B.; Pathirana, S.W.; Wood, S.; Singh, M.; Trang, B.T. Finite Element Analysis of Demountable Steel-Concrete Composite Beams under Static Loading. Adv. Steel Constr. 2018, 14, 392–411, doi:10.18057/IJASC.2018.14.3.5.
[32] European Commitee for Standardization CEN, EN 1993-1-8: Eurocode 3: Design of steel structures—Part 1-8: Design of joints., 2005.